



ELSEVIER

Surface Science 321 (1994) L225–L232

surface science

## Surface Science Letters

A new type of reconstruction on the InSb( $\bar{1}\bar{1}\bar{1}$ ) surface determined by grazing incidence X-ray diffractionJ. Wever<sup>a</sup>, H.L. Meyerheim<sup>a,\*</sup>, W. Moritz<sup>a</sup>, V. Jahns<sup>a</sup>, D. Wolf<sup>a</sup>, H. Schulz<sup>a</sup>,  
L. Seehofer<sup>b</sup>, R.L. Johnson<sup>b</sup><sup>a</sup> Institut für Kristallographie und Mineralogie, Universität München, Theresienstrasse 41, 80333 München, Germany<sup>b</sup> II. Institut für Experimentalphysik, Universität Hamburg, Luruper Chaussee 149, 22761 Hamburg, Germany

Received 27 July 1994; accepted for publication 26 August 1994

**Abstract**

The  $(3 \times 3)$  reconstruction of the InSb( $\bar{1}\bar{1}\bar{1}$ ) surface has been investigated by grazing incidence X-ray diffraction and scanning tunneling microscopy. The structure is characterized by 6-atom rings on top of a slightly buckled InSb top double layer. Two types of rings have been found, an elliptic ring consisting of 4 In and 2 Sb atoms and a trigonal ring with 3 In and 3 Sb atoms. The bond angles and lengths are consistent with the concept of rehybridization and depolarization which explains the reconstructions of the (111) and (110) surfaces.

The surfaces of III/V semiconductors exhibit a number of complex reconstructions. The driving force behind these reconstructions can be explained in terms of orbital rehybridization and depolarization of the surface. This is in contrast to the elemental semiconductors where one usually assumes that the minimization of the number of dangling bonds is the dominant factor. On the polar (111) and ( $\bar{1}\bar{1}\bar{1}$ ) surfaces the stoichiometry is an additional parameter which can be influenced by the preparation of the surface. The  $(2 \times 2)$  reconstructions of GaAs, GaSb, GaP and InSb have been studied by low energy electron diffraction (LEED) [1,2], X-ray diffraction (XRD) [3,4] and scanning tunneling microscopy (STM) [5]. They are very similar and the rehybridization is associated with Ga or In vacancies. In addition,

for InSb(111) and GaAs(111) a certain density of Sb or As vacancies seems to exist [6]. On the ( $\bar{1}\bar{1}\bar{1}$ ) surfaces vacancies are not expected because the As or Sb dangling bonds are less energetic than the dangling bonds of In or Ga [7].

Very little is known about the ( $\bar{1}\bar{1}\bar{1}$ ) surfaces. In general they are less stable than the (111) surfaces and exhibit a number of structures depending on the surface composition. For GaAs( $\bar{1}\bar{1}\bar{1}$ ) a variety of superstructures has been found with varying As concentration [8–10]. A number of models have been proposed, namely a trimer model [11], a multivacancy model [12] for the  $(2 \times 2)$  phase, and a staggered As vacancy model for the  $(\sqrt{19} \times \sqrt{19})$ -R23.4°-phase [13]. Recently, a two layered hexagonal ring structure consisting of 12 atoms has been derived from STM measurements for the latter [11]. For InSb( $\bar{1}\bar{1}\bar{1}$ ) a  $(3 \times 3)$  superstructure has been found after annealing under UHV conditions. After evapo-

\* Corresponding author. Fax: +49 89 2394 4334.

ration of Sb a  $(2 \times 2)$  reconstruction can be stabilized. None of the reconstructions of the  $(\bar{1}\bar{1}\bar{1})$  surfaces could be uniquely determined. Photoemission studies of the  $\text{InP}(\bar{1}\bar{1}\bar{1})$ - $(2 \times 2)$  phase indicated small relaxation in the top layers [14] and a transmission electron microscopy study of the  $\text{InSb}(\bar{1}\bar{1}\bar{1})$ - $(2 \times 2)$  surface confirmed the trimer model [15].

We present here a new model for the  $(3 \times 3)$  reconstruction which differs from all structures observed until now on semiconductor surfaces. A statistical random mixture of two types of rings having a lower symmetry than the substrate and occurring in different orientations is the most important feature of this superstructure. There is evidence for In–In bonds in one type of 6-atom rings and the stoichiometry of the surface is changed toward a depletion of Sb.

The  $(3 \times 3)$  reconstruction was prepared in ultra high vacuum (UHV) by several cycles of  $\text{Ar}^+$  ion bombardment at 500 K followed by subsequent annealing at 673 K for several hours and slow cooling to room temperature (RT) at 2 K/min. During the XRD measurements in UHV (base pressure  $< 4 \times 10^{-10}$  mbar) the surface was stable for several days, whereas it was unstable under the electron beam. Data collection was performed at the W1 beam line of the Hamburger Synchrotron Radiation Laboratory HASYLAB at  $1.0^\circ$  X-ray incidence angle using a wavelength of 1.361 Å. In total 278 symmetrically independent reflections were measured consisting of 71 in-plane and 207 out of plane reflections along 24 superstructure lattice rods. A maximum beam exit angle of  $70^\circ$  corresponding to  $q_z = 0.64 \text{ \AA}^{-1}$  could be achieved with our diffractometer. This is equivalent to  $l = 8.2$  reciprocal lattice units. After correcting the data for active sample area, polarization- and Lorentz-factor [16] the Patterson function  $P(uv0)$  [17] was calculated showing the interatomic vectors of the structure projected along  $z$ . Using the in-plane ( $q_z \approx 0$ ) data only was not sufficient to derive a trial structure model. Only the complete data set allowed to calculate sections through the 3D Patterson function. In this case no information is lost by the superposition of positive and negative densities by the projection. The 3D Patterson function together with the STM images were the key to solve the structure. Two Patterson sections parallel (at  $w = 0$ ) and normal (at  $u = 0$ ) to the surface are plotted in Fig. 1, where the interatomic vectors within the

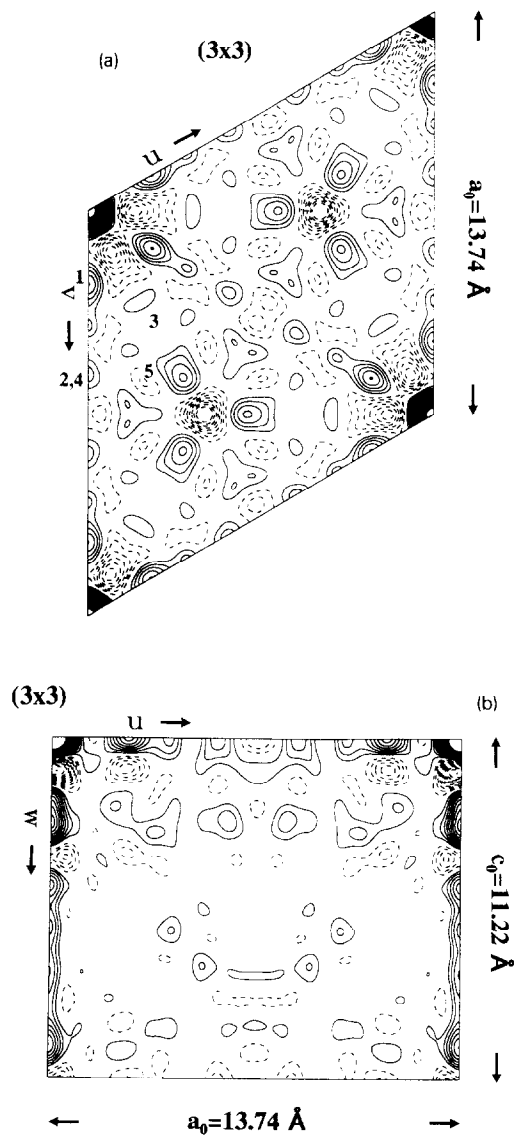


Fig. 1. (a) Patterson section  $P(uv0)$  parallel to the surface of the  $(3 \times 3)$  unit cell. Solid and dashed lines indicate positive and negative maxima, respectively. Some positive maxima are labeled by 1–5. (b) Patterson section  $P(u0v)$  normal to the surface.

$(3 \times 3)$  unit cell ( $a_0 = b_0 = 13.74 \text{ \AA}$ ,  $c_0 = 11.22 \text{ \AA}$ ) are given by solid lines. Negative maxima (dashed lines) also appear since only superlattice reflections were included in the calculation [18]. The Patterson sections show that the main features of the reconstruction are in the surface plane, and that only a small number of symmetrically independent inter-

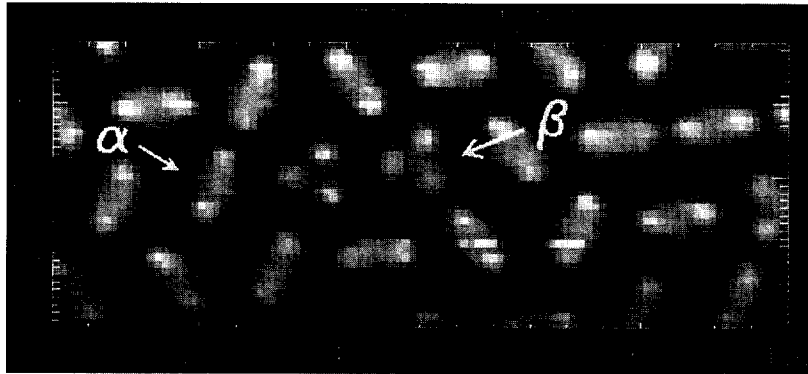


Fig. 2. STM topograph of a  $100 \times 40 \text{ \AA}^2$  area of the  $3 \times 3$ -phase of  $\text{InSb}(\bar{1}\bar{1}\bar{1})$  recorded at  $+0.7 \text{ V}$  sample bias and  $2.4 \text{ nA}$  tunnel current. The corrugation is  $0.2 \text{ \AA}$ . The elliptic and trigonal types of 6-atom rings shown in Fig. 4 are marked by  $\alpha$  and  $\beta$ . The bright spots at the rings correspond to Sb atoms.

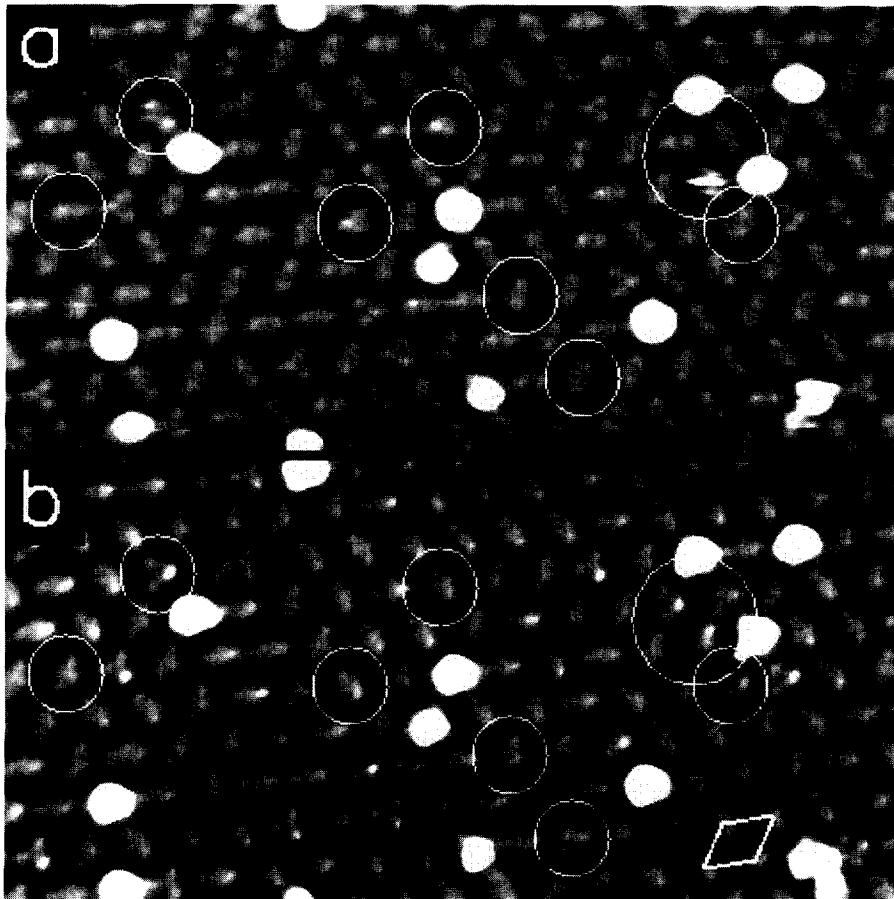


Fig. 3. Two topographs (a and b) of the same area  $200 \times 100 \text{ \AA}^2$  taken at 15 min time difference. The circles indicate an elliptic ring changing orientation with time (outer left side) and distorted trigonal features ( $\gamma$ -ring, see also Fig. 4). Large bright spots are possibly due to impurity atoms. In the lower right part of 3b one  $(3 \times 3)$  unit cell is marked.

atomic vectors exists parallel to the surface plane. Therefore, only a small number of atoms are expected in the asymmetric unit. The Patterson section at  $w = 0$  is consistent with ring-like structures, all other models which had been tried generated more maxima in the Patterson function [19]. For the in plane Patterson function  $P(uv0)$  we have indicated several maxima labeled by 1–5 which can be correlated with interatomic vectors within the rings as well as between the rings. This will be discussed in more detail below. Further, a strong intensity variation along  $q_z$  is observed which cannot be explained by a simple adatom or vacancy structure but is indicative for additional relaxations in deeper layers.

STM topographs were recorded in a separate system on samples prepared by using the same procedure [20]. We were only able to achieve atomic resolution for negative sample bias. For positive sample bias the tunneling conditions turned out to be extremely unstable which corresponds presumably to the faceting observed with LEED. The STM images shown in Fig. 2 reveal the  $(3 \times 3)$  superstructure to be composed of elongated structures ( $\alpha$ ) having three different  $120^\circ$  rotated orientations and of trigonal structures ( $\beta$ ) having two different  $180^\circ$  rotated orientations.

These structures are packed in a random distribution. The individual units were found to rotate at RT indicating weak interaction between neighbouring units. In Figs. 3a and 3b we show two  $200 \times 100 \text{ \AA}^2$  STM topographs which were recorded at 15 min time difference. The circles mark specific features. First, at the outer left side an elliptic ring is observed that changes its orientation. The other circles indicate distorted trigonal features which we call  $\gamma$ -ring (see also Fig. 4). It can be attributed to an intermediate state during the rotation of an  $\alpha$  ring. The large bright spots are possibly due to impurities. However, both features, the  $\gamma$ -ring and the impurities cover less than 10% of the surface area.

The results discussed so far allowed to derive a variety of models which have been tried to refine. The only model for which an unweighted residuum  $R_w$  below 0.25 could be achieved is shown in Fig. 4. The structure consists of two types of six-atom rings on top of a complete InSb double layer. The fraction of the trigonal rings is about 7% which is in reasonable agreement with the STM picture which showed

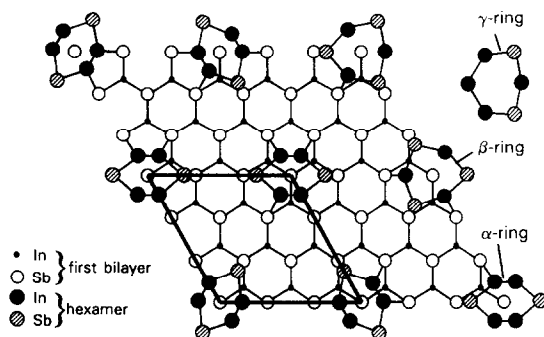


Fig. 4. Top view of the structure model, the solid line indicates the  $(3 \times 3)$  unit cell. The  $\gamma$ -ring is an intermediate state of the  $\alpha$ -ring changing its orientation and corresponds to the encircled triplets in Fig. 3.

a concentration of about 10%. On the basis of the X-ray data it is not possible to distinguish between In and Sb atoms due to their almost identical scattering power. The assignment of the different sites to In or Sb follows therefore from the observed bond geometry and also from the STM pictures where the dangling bonds of Sb appear as small bright spots at the trigonal and elliptic rings. The rehybridisation from  $sp^3$  to  $sp^2$  orbitals for the group III elements is connected with a change of the bond angles towards a planar three-fold coordination which is observed for four atoms in the elliptic ring. For the other two atoms the bond angles become smaller which can be understood by a rehybridisation from  $sp^3$  to  $sp_{xyz}$  bonds which occurs for the group V elements. The bond geometry apparently approaches trigonal flat and rectangular configurations which we assign to In and Sb atoms, respectively.

It is important to note that the  $(3 \times 3)$  unit cell is only obtained by averaging over the different ring orientations. Due to the local  $mm2$  and  $3m$  symmetry of the rings there are only two symmetrically independent atoms per ring. The structure analysis proceeded with successive refinement of the free parameters. In the final step 50 adjustable parameters were refined, 46 position parameters, 1 overall temperature factor, two scale factors for in-plane and out of plane data, respectively and 1 occupancy factor for the mixture of the trigonal and elliptic rings. Different scale factors had to be used because the out of plane data were measured with a higher  $q_z$  resolution than the in plane data. The different ring orienta-

tions were treated by using split positions for the atoms. Split positions and anisotropic temperature factors have been tried to take account of relaxations in the first InSb double layer according to the orientation of the rings. However, no significant improvement of the fit quality could be achieved.

In spite of the complexity of the superstructure when describing it in detail including the atomic shifts within the first three InSb double layers, the main vectors within the ring structure show up directly in the Patterson sections, although there is some overlap between different vectors. For example, in Fig. 1a the positive maxima labeled 1 can be correlated with the short In–In interatomic vectors ( $\approx 2.4 \text{ \AA}$ ) within the  $\alpha$  rings shown in Fig. 4. Further, the short vector (3.02  $\text{\AA}$ ) between the In and the Sb atoms in the  $\alpha$  rings can be related to maximum 3, whereas the long Sb–Sb interatomic vectors within the  $\alpha$  and the  $\beta$  ring correspond to the maxima labeled 4 and 5, respectively. It should be noted that the maximum 4 can also be interpreted by the diagonal In–In vector between the two opposite In atom pairs of the  $\alpha$  ring. As a result of this overlap the position of the maximum 2,4 does not

exactly correspond to the lengths of the interatomic vectors in this case. Finally, the strong maximum 5 (and the symmetry equivalent maxima) can also be interpreted by interatomic vectors between different rings.

For the best fit model we obtained a weighted ( $R_w$ ) and unweighted ( $R_u$ ) residual [21] of 0.048 and 0.15, respectively. The ‘‘goodness of fit’’ (GOF) of 1.1 was obtained indicating that the agreement between observed and calculated intensities is within the experimental uncertainty [17]. For example we show in Fig. 5 the agreement between measured and calculated intensities for four superstructure rods. In total 24 superstructure rods have been fitted, all with similar accuracy. An agreement of that quality is indicative that the structure model is correct.

Models of the two types of rings are shown in Fig. 6. The bond lengths and bond angles within the rings as well as between the ring atoms and the top layer atoms are given in Table 1. The Table 2 lists the relative coordinates of the atoms within the rings and in the first three double layers. In addition, for the latter, the lateral and vertical shifts of the atoms from their bulk positions are given in  $\text{\AA}$ .

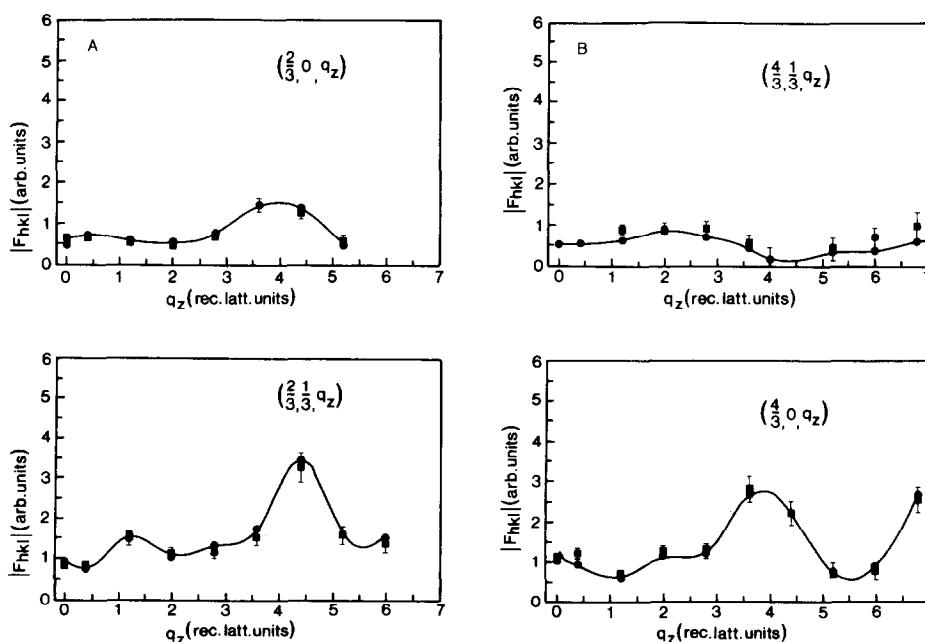


Fig. 5. Observed (squares) and calculated (full circles) structure factors of superstructure lattice rods. The full line is drawn to guide the eye.

Table 1

Derived bond lengths (Å) and angles between ring atoms and first double layer atoms (see also Fig. 6)

	In–In (within ring)	In–Sb (within ring)	In–Sb (to double layer)	Sb–Sb (to double layer)	$\alpha_{\text{Sb}}$	$\beta_{\text{Sb}}$	$\alpha_{\text{In}}$	$\beta_{\text{In}}$	$\gamma_{\text{In}}$
$\alpha$ ring	2.31	3.02	2.89	2.75	80.2°	94.6°	136.8°	106.4°	111.9°
$\beta$ ring	–	3.01	2.71	2.77	94.2°	96.8°	137.2°	110.7°	–

Some important features of the of the structure can be summarized as follows:

- (i) The In–In distances occurring in the elliptic ring, 2.31 Å, are significantly smaller than the bulk value of the In–Sb bond length of 2.75 Å and much smaller than the In–In distance in bulk In which is 3.24 Å. The In–Sb distances are in both rings larger than in the bulk while the bond lengths to the Sb atoms of the top

layer are approximately the same as in the bulk. The short In–In distance of 2.31 Å may be explained by a some ionicity of the In atoms as a result of charge transfer to the Sb atoms. This is in agreement with the concept of rehybridization of the surface In and Sb atoms discussed above. According to Shannon and Prewitt [22] the effective radius for  $\text{In}^+$  is 1.30 Å for six-fold coordination which corre-

Table 2

Atomic positions in the adatom rings and in the top three double layers

		Relative coordinates			Shift from bulk position	
		x	y	z	Lateral	Vertical
$\alpha$ ring	Sb	0.250(3)	0.246(3)	–0.236(4)	–	–
	In	0.167(2)	0.166(2)	–0.176(3)	–	–
$\beta$ ring	Sb	0.228(3)	0.228(3)	–0.232(5)	–	–
	In	0.187(3)	0.187(3)	–0.191(5)	–	–
1. double layer	Sb1	0.000	0.000	0.029(4)	–	0.32(4)
	Sb2	0.666	0.333	–0.073(4)	–	–0.82(4)
	Sb3	0.333	0.666	–0.004(4)	–	–0.05(5)
	Sb4	0.325(1)	0.325(1)	–0.009(3)	0.11(1)	0.10(3)
	In5	0.230(2)	0.115(1)	0.109(3)	0.10(2)	0.29(3)
	In6	0.565(1)	0.45(19)	0.044(3)	0.22(1)	0.44(3)
	In7	0.218(1)	0.436(2)	0.087(3)	0.10(2)	0.04(3)
2. double layer	Sb8	0.222(2)	0.111(1)	0.354(3)	0.00(2)	0.23(3)
	Sb9	0.557(1)	0.443(1)	0.304(3)	0.03(1)	–0.33(3)
	Sb10	0.221(1)	0.442(2)	0.318(2)	0.02(2)	–0.17(3)
	In11	0.454(2)	0.227(1)	0.390(3)	0.12(2)	–0.30(5)
	In12	0.448(2)	0.552(1)	0.388(3)	0.09(2)	–0.33(5)
	In13	0.112(1)	0.224(2)	0.410(3)	0.02(2)	–0.08(5)
3. double layer	Sb14	0.452(2)	0.226(1)	0.649(5)	0.09(2)	–0.19(6)
	Sb15	0.446(1)	0.554(1)	0.638(5)	0.03(2)	–0.32(6)
	Sb16	0.112(1)	0.224(2)	0.660(5)	0.01(2)	–0.07(6)
	In17	0.000	0.000	0.752(7)	–	0.02(6)
	In18	0.667	0.333	0.762(7)	–	0.14(8)
	In19	0.333	0.667	0.736(7)	–	–0.15(8)
	In20	0.337(2)	0.337(2)	0.750(7)	0.05(2)	0.00(8)

The local point symmetry of the 6 atom rings has been assumed to be  $mm2$  and  $3m$  with two symmetrically independent atoms per ring. The lattice constants are  $a = 13.74$  Å and  $c = 11.22$  Å, hexagonal setting of the unit cell.

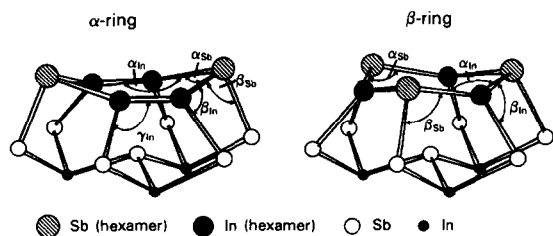


Fig. 6. Perspective view of the elliptic  $\alpha$ -ring and the trigonal  $\beta$ -ring. The bond angles and bond lengths are given in Table 1.

sponds to a minimum bond length of 2.60 Å. Keeping in mind that the effective radii decrease with decreasing coordination number a minimum distance of 2.31 Å still appears to be reasonable. In this context it should be noted that an interatomic vector of 2.3–2.4 Å is directly evident in the Patterson section  $P(uv0)$ .

- (ii) The lateral shifts are as large as 0.22 Å in the top layer but damp out in the second and third layer. One might expect an influence of the different ring orientations on the lateral shifts of the atoms of the first double layer. However, using split positions for the atoms in the first double layer in order to represent the induced disorder, no significant improvement of the fit could be achieved. The maximum vertical shift is 0.8 Å. The atom Sb3 at (1/3, 2/3) is shifted outward by about 0.8 Å so that smaller bond angles result. The atom Sb2 at (2/3, 1/3) exhibits only a slight outward displacement by 0.05 Å. It seems possible to assign this position also to an In atom.
- (iii) It is interesting to note that the structure does not satisfy the autocompensation ansatz which expects that all dangling bonds are filled on surface anions and empty on surface cations [23,24]. If we neglect the fraction of the trigonal rings there remain 4 In and 5 Sb dangling bonds per unit cell, which means that the Sb dangling bonds are filled on the average with 1.85 electrons, or, alternatively, all but one of the Sb dangling bonds are filled with two electrons and one remains with 5/4 electrons. This may explain why the two Sb atoms at (2/3, 1/3) and (1/3, 2/3) behave differently.

The atom Sb3 at (1/3, 2/3) exhibits only a slight relaxation indicating a partial rehybridisation. The deviation from autocompensation may be understood by the consideration that the electron counting rule cannot be fulfilled with a (3 × 3) periodicity and the surface comes to it as close as possible,

The reconstructions of the (110) and (111) surfaces of several III/V semiconductors have been found to be similar. It is therefore likely that the structure model presented here applies also to the (3 × 3) reconstruction of GaAs (111) and with slight modifications to the more complex patterns observed on other (111) surfaces of the III/V semiconductors.

### Acknowledgements

The financial support of the Volkswagen Stiftung under project No. I/65 092 and of the Bundesministerium für Forschung und Technologie (BMFT) under No. 05 WM5IBB8 and project No. 05 5GUABI are gratefully acknowledged.

### References

- [1] S.Y. Tong, G. Xu and W.N. Mei, Phys. Rev. Lett. 52 (1984) 1693.
- [2] G. Xu, W.Y. Hu, J.L. Yeh and S.R. Wang, Phys. Rev. B 32 (1985) 8473.
- [3] J. Bohr, R. Feidenhans'l, M. Nielsen, M. Toney, R.L. Johnson and I.K. Robinson, Phys. Rev. Lett. 54 (1985) 1275.
- [4] R. Feidenhans'l, M. Nielsen, F. Grey, R.L. Johnson and I.K. Robinson, Surf. Sci. 186 (1987) 499.
- [5] A.W. Haberen and M.B. Pashley, Phys. Rev. B 41 (1990) 3226.
- [6] A. Belzner, E. Ritter and H. Schulz, Surf. Sci. 209 (1989) 379.
- [7] D.J. Chadi, Phys. Rev. Lett. 52 (1984) 1911.
- [8] K. Jacobi, C. von Muschwitz and W. Ranke, Surf. Sci. 82 (1979) 270.
- [9] M. Alonso, F. Soria and J.L. Sacedon, J. Vac. Sci. Technol. A 3 (1985) 1598.
- [10] R.D. Bringans and R.Z. Bachrach, Phys. Rev. Lett. 53 (1984) 1954.
- [11] D.K. Biegelsen, R.D. Bringans, J.E. Northrup and L.-E. Swartz, Phys. Rev. Lett. 65 (1990) 452.
- [12] D.J. Chadi, Phys. Rev. Lett. 57 (1986) 102.
- [13] E. Kaxiras, Y. Bar-Yam, J.D. Jannopoulos and K.C. Pandey, Phys. Rev. Lett. 57 (1986) 106; Phys. Rev. B 35 (1987) 9625.

- [14] X. Hou, G. Dong, X. Ding and X. Wang, Surf. Sci. 183 (1987) 123.
- [15] T. Nakada and T. Osaka, Phys. Rev. Lett. 67 (1991) 2834.
- [16] C. Schamper, H.L. Meyerheim and W. Moritz, J. Appl. Cryst. 26 (1993) 687.
- [17] R. Feidenhans'l, Surf. Sci. Rep. 10 (1989) 105.
- [18] M.J. Buerger, Vector Space and its Applications in Crystal Structure Investigations (Wiley, New York, 1959).
- [19] J. Wever, Dissertation, Universität München (1994).
- [20] L. Seehofer, Dissertation, Universität Hamburg (1993).
- [21] The residua are given by  $R_u = \sum_{hkl} ||F_{hkl}^{obs}| - |F_{hkl}^{calc}|| / \sum_{hkl} |F_{hkl}^{obs}|$  and  $R_w = (\sum_{hkl} w_{hkl} ||F_{hkl}^{obs}| - |F_{hkl}^{calc}||^2 / \sum_{hkl} w_{hkl} |F_{hkl}^{obs}|^2)^{1/2}$ , with  $w_{hkl} = \sigma_{hkl}^{-2}$  and  $GOF = (N - p)^{-1} \sum_{hkl} (||F_{hkl}^{obs}| - |F_{hkl}^{calc}||^2 / \sigma_{hkl}^2)$ , where  $N$  is the number of reflections and  $p$  the number of free parameters.
- [22] R.D. Shannon and C.T. Prewitt, Acta Cryst. B 25 (1969) 925
- [23] M.D. Pashley, Phys. Rev. B 40 (1989) 10481.
- [24] W. Mönch, Semiconductor Surfaces and Interfaces (Springer, Berlin, 1993).